AGU PUBLICATIONS

JGR

Journal of Geophysical Research: Oceans

RESEARCH ARTICLE

10.1002/2017JC013052

Impacts of the Tropical Pacific Cold Tongue Mode on ENSO Diversity Under Global Warming

Yang Li[1], Jianping Li[2,3], Wenjun Zhang[4], Quanliang Chen[1], Juan Feng[2], Fei Zheng[5], Wei Wang[1], and Xin Zhou[1]

[1]College of Atmospheric Science, Plateau Atmosphere and Environment Key Laboratory of Sichuan Province, Chengdu University of Information Technology, Chengdu, China, [2]State Key Laboratory of Earth Surface Processes and Resource Ecology and College of Global Change and Earth System Science, Beijing Normal University, Beijing, China, [3]Laboratory for Regional Oceanography and Numerical Modeling, Qingdao National Laboratory for Marine Science and Technology, Qingdao, China, [4]Collaborative Innovation Center on Forecast and Evaluation of Meteorological Disasters, Key Laboratory of Meteorological Disaster of Ministry of Education, Nanjing University of Information Science and Technology, Nanjing, China, [5]State Key Laboratory of Numerical Modeling for Atmospheric Sciences and Geophysical Fluid Dynamics (LASG), Institute of Atmospheric Physics, Chinese Academy of Sciences, Beijing, China

Key Points:
- The CTM is controlled by the vertical gradient of sea temperature anomaly through the ocean dynamical feedback under global warming
- The ENSO diversity in its spatial structure seems to be closely associated with the CTM
- The CTM is responsible for more frequent occurrence of CP-El Niño under global warming

Correspondence to:
J. Li,
ljp@bnu.edu.cn;
Q. Chen,
chenql@cuit.edu.cn

Citation:
Li, Y., Li, J., Zhang, W., Chen, Q., Feng, J., Zheng, F., . . . Zhou, X. (2017). Impacts of the Tropical Pacific Cold Tongue Mode on ENSO Diversity Under Global Warming. *Journal of Geophysical Research: Oceans*, *122*, 8524–8542. https://doi.org/10.1002/2017JC013052

Received 3 MAY 2017
Accepted 28 SEP 2017
Accepted article online 6 OCT 2017
Published online 7 NOV 2017

Abstract The causes of ENSO diversity, although being of great interest in recent research, do not have a consistent explanation. This study provides a possible mechanism focused on the background change of the tropical Pacific as a response to global warming. The second empirical orthogonal function mode of the sea surface temperature anomalies (SSTA) in the tropical Pacific, namely the cold tongue mode (CTM), represents the background change of the tropical Pacific under global warming. Using composite analysis with surface observations and subsurface ocean assimilation data sets, we find ENSO spatial structure diversity is closely associated with the CTM. A positive CTM tends to cool the SST in the eastern equatorial Pacific and warm the SST outside, as well as widen (narrow) zonal and meridional scales for El Niño (La Niña), and vice versa. Particularly in the positive CTM phase, the air-sea action center of El Niño moves west, resembling the spatial pattern of CP-El Niño. This westward shift of center is related to the weakened Bjerknes feedback (BF) intensity by the CTM. By suppressing the SSTA growth of El Niño in the eastern equatorial Pacific, the CTM contributes to more frequent occurrence of CP-El Niño under global warming.

1. Introduction

The El Niño-Southern Oscillation (ENSO), driven by ocean-atmosphere interaction in the tropical Pacific, is the most prominent interannual natural phenomenon with worldwide climate impacts. Great progress has been achieved in understanding ENSO dynamics in the past four decades (e.g., Battisti & Hirst, 1989; Bjerknes, 1969; Jin, 1997a, 1997b; Picaut et al., 1997; Suarez & Schopf, 1988; Wang, 2001; Weisberg & Wang, 1997; Wyrtki, 1975). Recently, attention of many studies turned into the issue of ENSO diversity, which represents the differences in the sea surface temperature (SST) pattern of ENSO event (e.g., Capotondi et al., 2015; Fedorov et al., 2015; Yu & Giese, 2013). For example, in terms of the differences in the location of the SST anomalies (SSTA) center over the tropical Pacific, the El Niño events could be distinguished two types, namely, the Eastern Pacific El Niño (EP-El Niño) and Central Pacific El Niño (CP-El Niño). Particularly, the CP-El Niño also referred to the dateline El Niño, El Niño Modoki, or warm pool El Niño, has occurred frequently since 1980s (e.g., Ashok et al., 2007; Kao & Yu, 2009; Karnauskas, 2013; Kug et al., 2009; Larkin & Harrison, 2005; Ren & Jin, 2011; Ren et al., 2013; Takahashi et al., 2011; Yeh et al., 2009). The CP-El Niño is characterized by maximum SSTA in the central equatorial Pacific, while the maximum SSTA in an EP-El Niño (also referred to as the conventional El Niño) is located in the eastern equatorial Pacific. Many studies have shown that the CP-El Niño gives rise to notably different features and climate impacts from EP-El Niño. For instance, the persistence barrier (e.g., Ren et al., 2016), and the impacts on East Asian climate (e.g., Feng & Li, 2011; Feng et al., 2016a, 2016b; Karori et al., 2013; Weng et al., 2007, 2009; Yuan & Yang, 2012; Zhang et al., 2011, 2013b, 2014), Australian autumn rainfall (e.g., Taschetto & England, 2009), Hadley cell (e.g., Feng & Li, 2013), and stratospheric climate (e.g., Garfinkel et al., 2013; Xie et al., 2012, 2014a, 2014b) have been discussed extensively. At present, the mechanisms associated with ENSO diversity are not well understood.

Recent studies suggested that extratropical Pacific climate variability plays an important role in ENSO diversity (e.g., Capotondi et al., 2015; Ding et al., 2015a, 2015b, 2015c; Feng et al., 2014; Larson & Kirtman, 2014; Yeh et al., 2015; Yu & Kim, 2011; Yu et al., 2010; Zhang et al., 2014). Yu et al. (2010) discussed that the CP-El Niño exhibits a strong connection to the subtropics of North Pacific. Based on the seasonal footprinting mechanism (e.g., Vimont et al., 2001, 2003a, 2003b), Yu and Kim (2011) further argued that the North Pacific Oscillation (NPO) could act as a bridge connecting the North Pacific region and CP-El Niño. Yeh et al. (2015) also stated that NPO-like atmospheric circulation is associated with the frequent occurrence of CP-El Niño, especially in the post-1990 period. Moreover, Ding et al. (2015c) proposed a relationship among ENSO diversity, NPO, and the Victoria mode (VM; Bond et al., 2003). They suggested that the linking mechanism is NPO→VM→ENSO, where the arrows show the cause-and-effect relationships. However, not all positive VM events are followed by a CP-El Niño event (Ding et al., 2015c). In addition, although there is a robust relationship between North Pacific meridional mode (NPMM) and ENSO, Larson and Kirtman (2014) found that NPMM shows promise as a predictor of EP-El Niño but less skill as a predictor of CP-El Niño. For the impact of the extratropical South Pacific climate variability on ENSO, Zhang et al. (2014) pointed out that the South Pacific meridional mode (SPMM) may be more effective in triggering EP-El Niño because the SPMM extends all the way to the eastern and central equatorial Pacific. These results suggested that there may be other factors responsible for ENSO diversity in addition to extratropical Pacific climate variability.

Some studies also documented that ENSO diversity is associated with the tropical Pacific background state (e.g., Ashok et al., 2007; Capotondi et al., 2015; Choi et al., 2011, 2012; Chung & Li, 2013; Collins et al., 2010; Xiang et al., 2013; Yeh et al., 2009). Yeh et al. (2009) noted that the greater occurrence of CP-El Niño under global warming is related to the background conditions, using observations and Coupled Model Intercomparison Project phase 3 (CMIP3) multimodel data sets. It is argued that a weakened Walker circulation associated with global warming is favorable for a flatter oceanic thermocline and thus more CP-El Niño events under global warming. However, a number of studies found that the long-term trend of tropical Pacific SSTA is characterized by cooling in the eastern equatorial Pacific and warming elsewhere in the tropical Pacific (e.g., Cane et al., 1997; Compo & Sardeshmukh, 2010; Funk & Hoell, 2015; Karnauskas et al., 2009; Solomon & Newman, 2012; Zhang et al., 2010). The corresponding strengthened Walker circulation, accelerated equatorial undercurrent (EUC), and accelerated subtropical cells (STCs) in the tropical Pacific have also been found in multiple observational data sets (e.g., Drenkard & Karnauskas, 2014; L'Heureux et al., 2013b; Yang et al., 2014). These observational results disagree with the speculation of Yeh et al. (2009). Therefore, it is necessary to further study the long-term trend of the tropical Pacific under global warming and its impacts on ENSO diversity.

Zhang et al. (2010) performed empirical orthogonal function (EOF) analysis of SSTA in the tropical Pacific using multiple SST data sets. It is worth mentioning that the EOF results are not sensitive to different SST reconstructions (Li et al., 2015; Zhang et al., 2010). The first EOF mode represents ENSO variability and the second EOF mode is identified as a cold tongue mode (hereafter CTM) (Figure 1). The CTM represents an out-of-phase relationship of SSTA variability between the Pacific cold tongue region and elsewhere in the tropical Pacific (Li et al., 2013; Zhang et al., 2010). A positive CTM is characterized by cold SSTA in the Pacific cold tongue region and warm SSTA in the rest of the tropical Pacific, with conditions reversed for a negative CTM. Note that the normalized principal component time series (NPC2) of the CTM exhibits a strong long-term trend (Figure 1). Specifically, the ocean dynamical processes are predominantly responsible for the long-term trend of the CTM in the tropical Pacific, where vigorous upwelling of cold water in the eastern equatorial region causes weaker warming in the eastern Pacific than in the western Pacific (Cane et al., 1997; Clement et al., 1996; Seager & Murtugudde, 1997; Sun & Liu, 1996; Zhang et al., 2010).

According to the quantitative analysis of heat budget equation, Li et al. (2015) further emphasized that the cooling from vertical advection of the anomalous temperature by the mean upwelling plays a major role in the long-term trend of the CTM, which is consistent with the results of DiNezio et al. (2009). This cooling advection term is controlled by the decreasing vertical gradient of the oceanic temperature anomaly (vertical axes is downward). Li et al. (2015) have depicted the ocean dynamical processes associated with the CTM in detail. Suppose a uniform external heating, which can be regarded as global warming, is imposed on the tropical Pacific. In the initial period, the SST will tend to increase, but the subsurface temperature is not affected. This leads the subsurface temperature toward a colder than surface temperature. In other words, the vertical gradient of the oceanic temperature anomaly ($\partial T'/\partial z$) is decreasing. Meanwhile, the

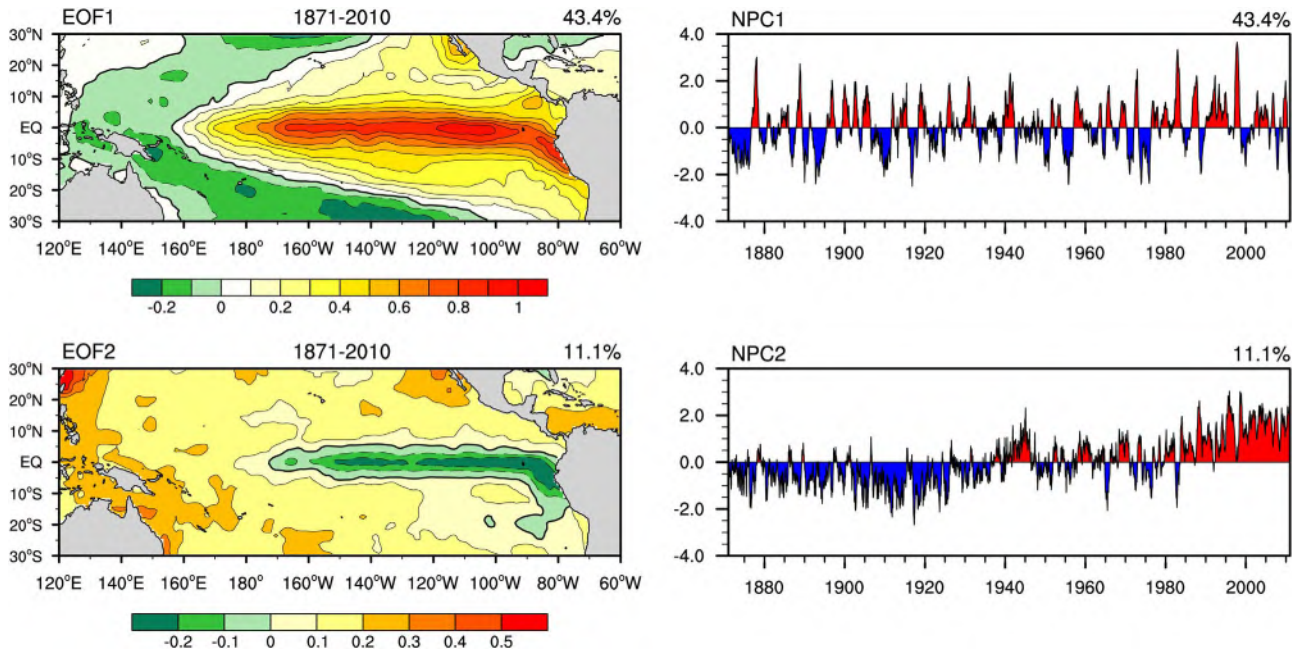

Figure 1. The spatial patterns and corresponding normalized PCs of the first two leading EOF modes of the tropical Pacific SST anomalies for the HadISST1 data set.

accompanying strong mean upwelling in the eastern equatorial Pacific could bring up colder subsurface water into surface layer. This corresponds to the cooling vertical advection of the anomalous temperature by the mean upwelling ($-\bar{w}\partial T'/\partial z$). As a result, it makes a contribution to the cooling ocean temperature anomaly, whose cooling center is located in the lower layer. This could further induce the decreasing term $\partial T'/\partial z$ in the eastern equatorial Pacific and thus enhance the cooling advection term $-\bar{w}\partial T'/\partial z$, which is thereby a negative feedback under global warming.

Zhang et al. (2010) and Li et al. (2015) have also pointed out that the CTM can well represent the long-term trend of the tropical Pacific under global warming. Meanwhile, the associated CTM pattern has also been reported in observations (e.g., Cane et al., 1997; Compo & Sardeshmukh, 2010; Funk & Hoell, 2015; Karnauskas et al., 2009; L'Heureux et al., 2013b; Solomon & Newman, 2012; Yang et al., 2014; Zhang et al., 2010). However, the long-term trend of the equatorial Pacific is still controversial. The first scientific question required to be answered is whether there is a cooling trend in the east, or not (e.g., Collins et al., 2010; Vecchi et al., 2008). To further verify the long-term trend of the equatorial Pacific under global warming, we will first confirm the long-term trend of oceanic temperature anomaly averaged from surface to subsurface (T') in the equatorial Pacific. Moreover, Li et al. (2015) have pointed out that the decreasing term $\partial T'/\partial z$ makes a major contribution to the long-term cooling trend of sea temperature of the equatorial Pacific through the ocean dynamical feedback associated with the CTM under global warming. Therefore, we will also investigate the long-term trend of the term $\partial T'/\partial z$, and reconfirm that the ocean dynamical feedback associated with the CTM is responsible for the long-term cooling trend of the eastern equatorial Pacific using multiple ocean reanalysis datasets. In addition, Duan et al. (2014) also showed that the CTM-like SSTA pattern could offset tendency errors in the simulation of the CP-El Niño in the Zebiak-Cane model (Zebiak & Cane, 1987). It is suggested that the background conditions provided by the CTM may have important impacts on ENSO diversity in its spatial pattern. However, this issue has not yet been discussed. In this paper, we will also discuss how the CTM affects ENSO diversity.

The rest of the paper is organized as follows. Section 2 gives a brief description of the observational data sets and methods. Section 3 first reconfirms the relationship between the CTM and the long-term trend of oceanic temperature in the equatorial Pacific, and then examines the impacts of the CTM on ENSO diversity and the associated air-sea interactions during the ENSO evolution period. Finally, conclusions and discussions are presented in section 4.

2. Data and Methodology

2.1. Data

The monthly SST from the Hadley Centre Sea Ice and SST data set version 1 (HadISST1) with a $1^\circ \times 1^\circ$ grid (Rayner et al., 2003) was used. Meanwhile, we used two relatively long-record temperature data sets to investigate the long-term trend of T' and $\partial T'/\partial z$ terms in the equatorial Pacific. The first was the Simple Ocean Data Assimilation product (SODA 2.2.4) with $0.5^\circ \times 0.5^\circ$ horizontal resolution and 40 vertical levels covering the period 1871–2010 (Carton & Giese, 2008). The second was the ECMWF Ocean Reanalysis System 4 product (ORAS4) with $1^\circ \times 1^\circ$ horizontal resolution and 42 vertical levels covering the period 1958–2010 (Balmaseda et al., 2013a, 2013b). The SODA 2.2.4 data set was also used to analyze the zonal wind stress and sea surface height anomaly (SSHA) in the present study. Because the CTM mainly exhibits a long-term trend, we used the long-term period (1871–2010), which is overlapping period for HadISST1 and SODA 2.2.4 data set, to study the impacts of the CTM on ENSO diversity. The mean seasonal cycle of all data sets from 1961 to 1990 has been removed. In addition, the NPC1 and NPC2 in Figure 1 are the normalized principal component time series of EOF1 and EOF2 of the tropical Pacific SSTA over the period 1871–2010, respectively.

2.2. Methodology

To quantify the influence of the CTM on ENSO meridional structure, an e-folding width of ENSO is applied based on previous studies (Zhang et al., 2009; Zhang & Jin, 2012, 2013a). This method first performs a zonal average (180°–90°W) of SSTA and then normalizes ENSO SSTA, dividing by the maximum SSTA in the central and eastern equatorial Pacific (3°S–3°N, 180°–90°W). We define the meridional width of ENSO as the distance from the equator to the latitude where the SSTA decreases to a threshold of zero. Note that the result of zero-threshold is consistent with that of 1/e-threshold. Meanwhile, the zonal width of the positive SSTA region along the equator (1°S–1°N, 120°E–90°W) is defined as the zonal width of El Niño. If the positive SSTA covers the entire equatorial Pacific, the zonal width is 150°. Otherwise, it is the width of positive SSTA in the central and eastern equatorial Pacific. This method is also applied to La Niña conditions. In addition, the EOF, composite analysis, and linear trend methods were used in our study. The significance of the trends was tested using the nonparametric Mann-Kendall method.

3. Results

3.1. Cooling Trend of Oceanic Temperature in the Eastern Equatorial Pacific

Figure 2 shows the long-term change of T' (averaged from surface to 60 m) in the equatorial Pacific based on two different data sets (i.e., SODA 2.2.4 and ORAS4). Here, a 7 year Gaussian low-pass filtering is applied to focus on the long-term change without ENSO signal. In spite of some differences, these two data sets exhibit similar sea temperature change in their overlapping period, such as the obvious equatorial oscillation and the alternating SSTA regimes (Figure 2). Especially in the SODA dataset, there is an overall cooling trend in the eastern equatorial Pacific and overall warming trend in the western equatorial Pacific. To reveal more clearly the long-term trends, Figure 4a shows the long-term trend of T' in the equatorial Pacific. In both SODA and ORAS4, there is a long-term cooling trend of T' in the eastern equatorial Pacific but warming trend of T' in the western equatorial Pacific (Figure 4a). The trends distribution of these two data sets during the post satellite era (Figure 4c) is consistent with that of their covering period (Figure 4a). Note that the trends of thermocline depth (20°C isotherm depth) anomalies shows a raising trend in the eastern equatorial Pacific during these two data sets covering period and the post satellite era (not shown). These results are consistent with Cane et al. (1997) and Solomon and Newman (2012). As the decreasing term $\partial T'/\partial z$ makes a major contribution to the long-term cooling trend of sea temperature of the eastern equatorial Pacific through ocean dynamical feedback associated with the CTM under global warming (DiNezio et al., 2009; Li et al., 2015), the long-term trend of the term $\partial T'/\partial z$ in the eastern equatorial Pacific is expected to be decreasing.

Figure 3 displays the long-term change of the term $\partial T'/\partial z$ in the equatorial Pacific. Clearly, the two data sets after filtering ENSO signal all depict a change of the term $\partial T'/\partial z$ from positive to negative in the eastern equatorial Pacific (Figure 3). Meanwhile, the SODA data set shows a decreasing trend of the term $\partial T'/\partial z$ in the eastern equatorial Pacific and an increasing trend of the term $\partial T'/\partial z$ in the western equatorial Pacific during the period 1871–2010 (Figure 4b). This trend distribution of SODA data set is more

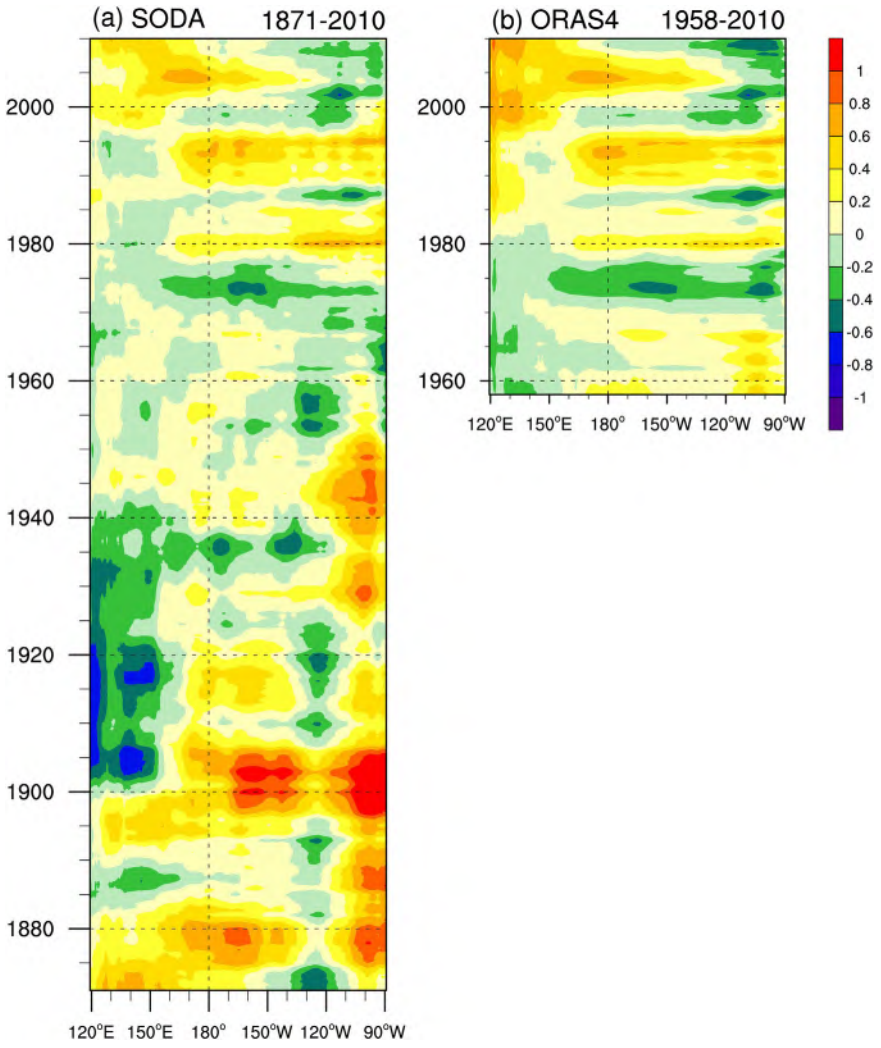

Figure 2. Time-longitude sections of monthly ocean temperature anomalies (from surface to 60 m; °C) averaged between 5°S and 5°N for (a) SODA 2.2.4 and (b) ORAS4, respectively. A 7 year Gaussian low-pass filter has been applied to the data.

obvious in the post satellite era (Figure 4d). Although the ORAS4 data set exhibits almost a decreasing trend of the term $\partial T'/\partial z$ in the equatorial Pacific during the period 1958–2010, the decreasing trend of the eastern equatorial Pacific is stronger than that of the western equatorial Pacific (Figure 4b). Especially for the post satellite era, the ORAS4 data set generally shows that there is a decreasing trend of the term $\partial T'/\partial z$ in the eastern equatorial Pacific but increasing trend of the term $\partial T'/\partial z$ in the western equatorial Pacific. To reiterate the ocean dynamical feedback associated with the CTM (Li et al., 2015), this decreasing term $\partial T'/\partial z$ accompanied by the mean upwelling could induce the cooling advection term $-\bar{w}\partial T'/\partial z$, which makes a contribution to the cooling ocean temperature in the eastern equatorial Pacific. Therefore, these results suggest that the decreasing $\partial T'/\partial z$ term, driven by global warming, is responsible for the long-term cooling trend in the eastern equatorial Pacific through the ocean dynamical feedback associated with the CTM. In addition, it is noted that these two data sets all show the remarkable negative $\partial T'/\partial z$ term over the period 1980–2010 (Figure 3). Interestingly, this period corresponds the frequent occurrence of CP-El Niño (e.g., Ashok et al., 2007; Kao & Yu, 2009; Kug et al., 2009; Larkin & Harrison, 2005; Yeh et al., 2009). Thus, an interesting question that needs to be addressed is, whether ENSO diversity is modulated by the CTM.

3.2. Impacts of the CTM on El Niño Diversity

To study the influence of the CTM on ENSO diversity, we first classify the ENSO and CTM events. Figure 5 shows the time series of NPC1 and NPC2 during boreal winter (from December to February, DJF). There is

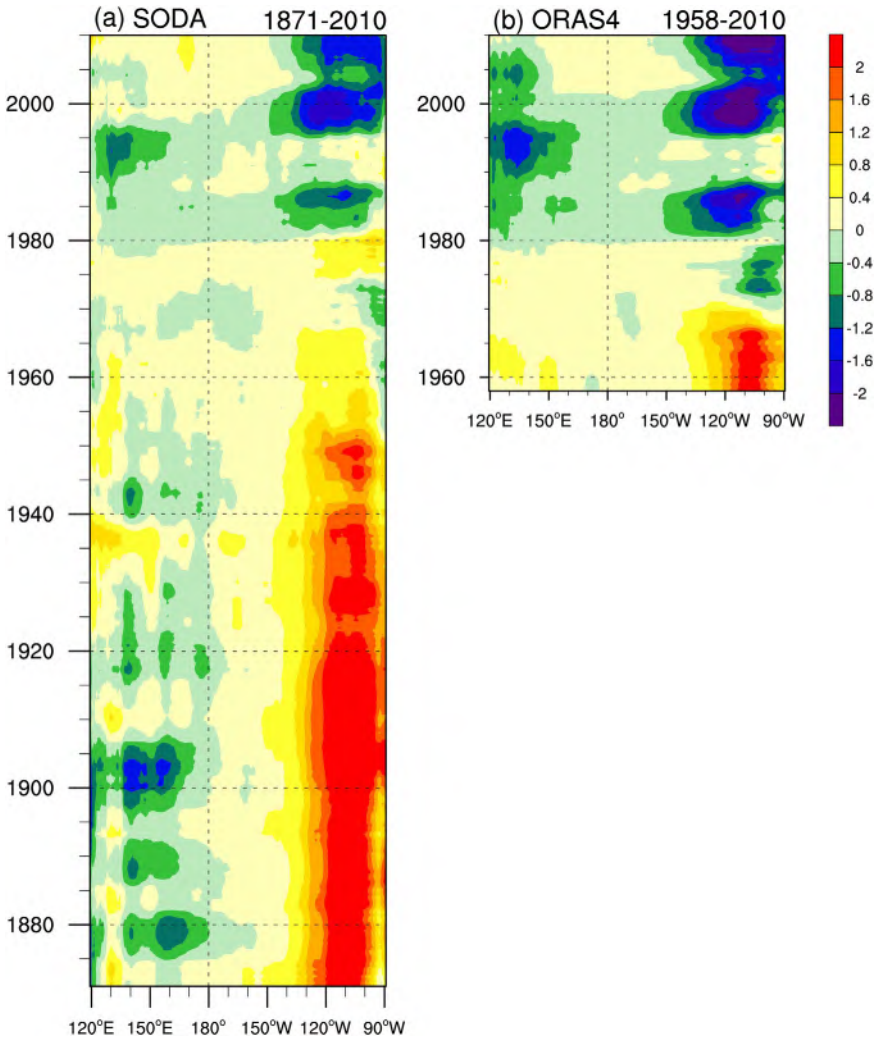

Figure 3. As in Figure 2, but for the vertical gradient of ocean temperature anomalies (10^{-2} °C m^{-1}).

an interannual variability in NPC1 and a long-term trend in NPC2 during boreal winter. The DJF-NPC2 is almost always negative before 1940, is dominated by interannual oscillation during the period 1940–1980, and is positive after 1980. On this basis, three periods (1871–1939, 1940–1979, and 1980–2010) will be considered in the following analysis. In addition, we identify ENSO events if the DJF-NPC1 value is greater than a half of its corresponding standard deviation (±0.5 SD). This approach is also used to distinguish positive and negative CTM (±CTM). Other years are defined as normal CTM (NCTM) events. According to these different categories, three classes for El Niño and for La Niña are identified as shown in Tables 1 and 2, respectively. These classes are labeled El Niño & −CTM, El Niño & NCTM, and El Niño & +CTM, and similarly for La Niña.

As shown in Table 1, the El Niño & −CTM class occurs most frequently before 1940, and the El Niño & NCTM class appears in all three periods, and the El Niño & +CTM class only occurs after 1940. Moreover, all events in the El Niño & +CTM class are CP-El Niño events (e.g., Ashok et al., 2007; Kao & Yu, 2009; Kug et al., 2009; Wang & Wang, 2013; Yu & Kim, 2013; Zhang et al., 2011, 2013b, 2014), except for the 1976 event. Particularly, over the period 1980–2010, all events in this class are CP-El Niño events. This is consistent with Ashok et al. (2007), who emphasized that the number of El Niño Modoki (i.e., CP-El Niño) events has increased since the early 1980s. These results motivate us to examine further the spatial properties of these three El Niño classes.

Figures 6a and 6b show that the composite distributions of El Niño & −CTM and El Niño & NCTM classes depict a typical ENSO horseshoe spatial pattern, which is similar to the conventional El Niño. However, the

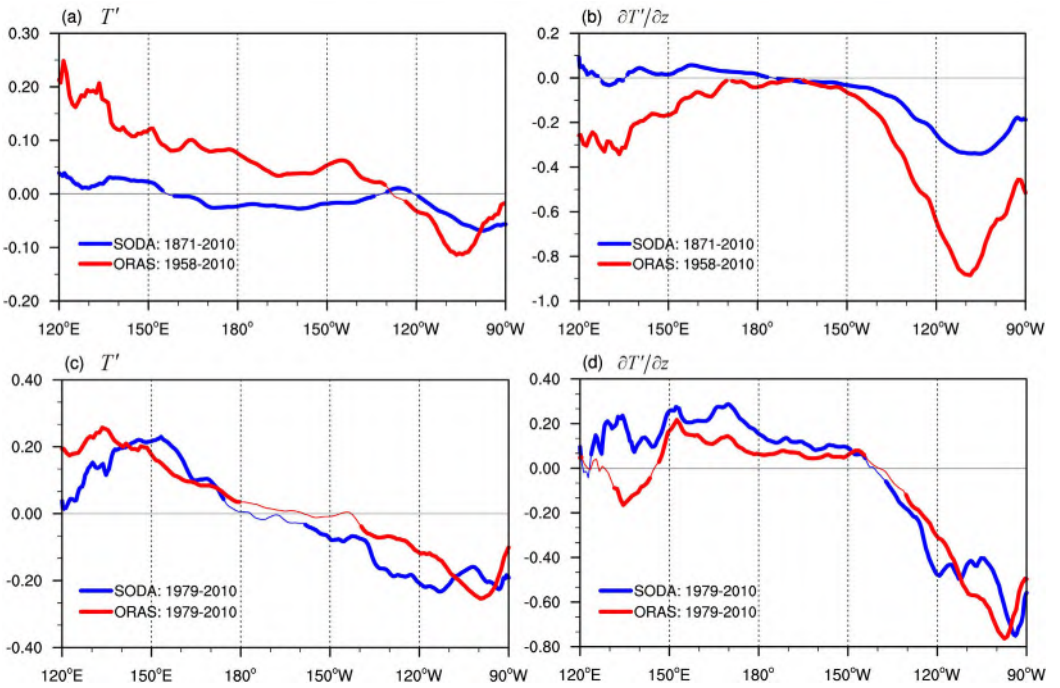

Figure 4. (a) The trends (in °C per 10 years) of ocean temperature anomalies in the equatorial Pacific (5°S–5°N, from surface to 60 m) for SODA 2.2.4 and ORAS4 data sets. (b) As in Figure 4a, but for the vertical gradient of ocean temperature anomalies (in °C m^{-1} per 1,000 years). (c) and (d) As in Figures 4a and 4b, but for the post satellite era (1979–2010). The blue and red lines represent the SODA and ORAS4 data sets, respectively. Thicker lines indicate significant at the 99% confidence level (nonparametric Mann-Kendall test).

El Niño & +CTM class is different from the others, with warming SSTA in almost the whole tropical Pacific (Figure 6c). In addition, its center is located in the central tropical Pacific, similar to that of CP-El Niño (Figure 6c). To more clearly distinguish the spatial differences between these three El Niño classes, we investigate their equatorial and off-equatorial SSTA, zonal and meridional structure, and center location in Figure 7. It is noted that Figure 7 is based on the composites in Figure 6.

Considering the cooling response of the eastern equatorial Pacific and warming response of outside the eastern equatorial Pacific to global warming (e.g., Cane et al., 1997; Zhang et al., 2010), we use SSTA averages in four areas (Figure 6b) to study the influence of the CTM on the equatorial and off-equatorial SSTA: the eastern equatorial area or Niño three area (A: 5°S–5°N, 150°W–90°W), the western equatorial area (B: 5°S–5°N, 120°E–180°E), and two off-equatorial areas (C: 10°N–30°N, 150°E–90°W; D: 10°S–30°S, 150°E–90°W).

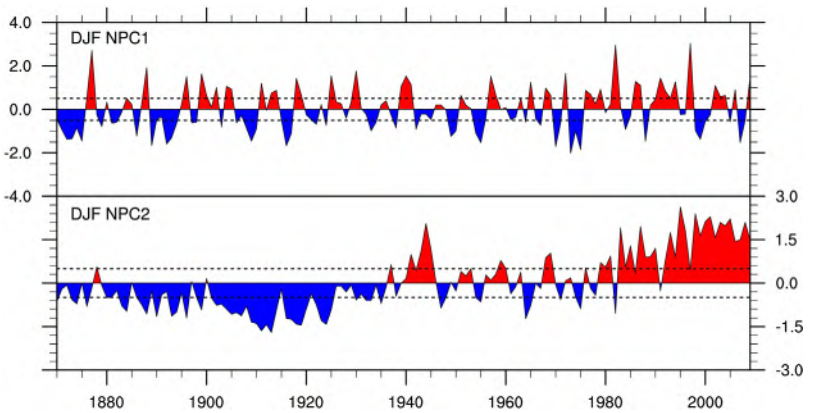

Figure 5. Time series of boreal winter (DJF) NPC1 and NPC2. The dotted lines denote their corresponding 0.5 SD.

Table 1
Classification of El Niño Years Into Three Types According to the Phase of the CTM for the Three Periods Considered Using Boreal Winter (December to February) Data

	Three types of El Niño		
Period	El Niño & −CTM	El Niño & NCTM	El Niño & +CTM
1871–1939	1876, 1888, 1896, 1899, 1902, 1904, 1905, 1911, 1913, 1914, 1918, 1919, 1925, 1930	1877, 1900, 1939	
1940–1979	1965	1940, 1951, 1957, 1958, 1963, 1972, 1977	1941, 1968, 1969, 1976, 1979
1980–2010	1982	1986, 1991, 1997	1987, 1992, 1993, 1994, 2002, 2003, 2004, 2006, 2009

Note that the cooling of the eastern equatorial SSTA and the warming of the off-equatorial SSTA from the El Niño & −CTM to El Niño & +CTM class is shown in Figure 7a. This warming off-equatorial SSTA is favorable for the widening of the meridional width from the El Niño & −CTM to El Niño & +CTM class (Figure 7b). Meanwhile, the decreased eastern equatorial SSTA in the El Niño & +CTM class shifts the air-sea action center for El Niño farther west, into the central equatorial Pacific (Figures 6c and 7c). In contrast, the centers of the El Niño & NCTM and El Niño & −CTM classes remain in the eastern equatorial Pacific (Figure 7c). Note also, the warming of the western equatorial Pacific SSTA from the El Niño & −CTM to El Niño & +CTM class is shown in Figure 7a. Correspondingly, the zonal width is gradually wide from the El Niño & −CTM to El Niño & +CTM class (Figure 7b).

The above results suggest that the spatial patterns of these three El Niño classes are very likely modified by the different CTM phase. Here we provide an alternative explanation to the impact of the CTM on El Niño spatial pattern. If a normal or neutral CTM is superposed on El Niño, the spatial pattern of El Niño should retain its natural structure (Figure 6b). This is supported by the strong spatial correlation coefficient (0.94) between the EOF1 pattern (Figure 1) and El Niño & NCTM. It implies that the impact of a normal CTM on El Niño can be ignored. Figures 7a and 7b also show that all the spatial characteristics in the El Niño & NCTM class remain in a normal state. When a negative CTM is superposed on El Niño, the eastern equatorial warming SSTA in the CTM may increase the eastern equatorial SSTA of El Niño (Figure 7a). Correspondingly, the center of El Niño remains in the eastern equatorial Pacific (Figure 7c). Similarly, the western equatorial and off-equatorial SSTA of El Niño could decrease (Figure 7a), because the cooling SSTA of the negative CTM is superposed on El Niño outside the eastern equatorial Pacific. This is favorable for the narrower zonal and meridional widths of El Niño (Figure 7b). In contrast, if a positive CTM is superposed on El Niño, the eastern equatorial cooling SSTA in the CTM could weaken the eastern equatorial SSTA of El Niño (Figure 7a) leading to a westward spreading of the El Niño center along the equator (Figures 6c and 7c). In addition, the warming SSTA of the positive CTM could modify the El Niño's SSTA structure by adding warming outside the eastern equatorial Pacific. That is, the positive CTM is favorable for the warming western equatorial and off-equatorial SSTA of El Niño (Figure 7a), which could broaden the zonal and meridional widths of El Niño (Figure 7b).

Table 2
Same as Table 1, *Except for La Niña*

	Three types of La Niña		
Period	La Niña & −CTM	La Niña & NCTM	La Niña & +CTM
1871–1939	1873, 1874, 1893, 1894, 1903, 1906, 1908, 1909, 1910, 1916, 1917, 1922, 1924, 1933	1871, 1872, 1875, 1879, 1881, 1882, 1886, 1889, 1892, 1897, 1898, 1934, 1938	
1940–1979	1954, 1955, 1964, 1971, 1975	1942, 1949, 1950, 1967, 1970, 1973, 1974	
1980–2010			1984, 1988, 1998, 1999, 2000, 2005, 2007

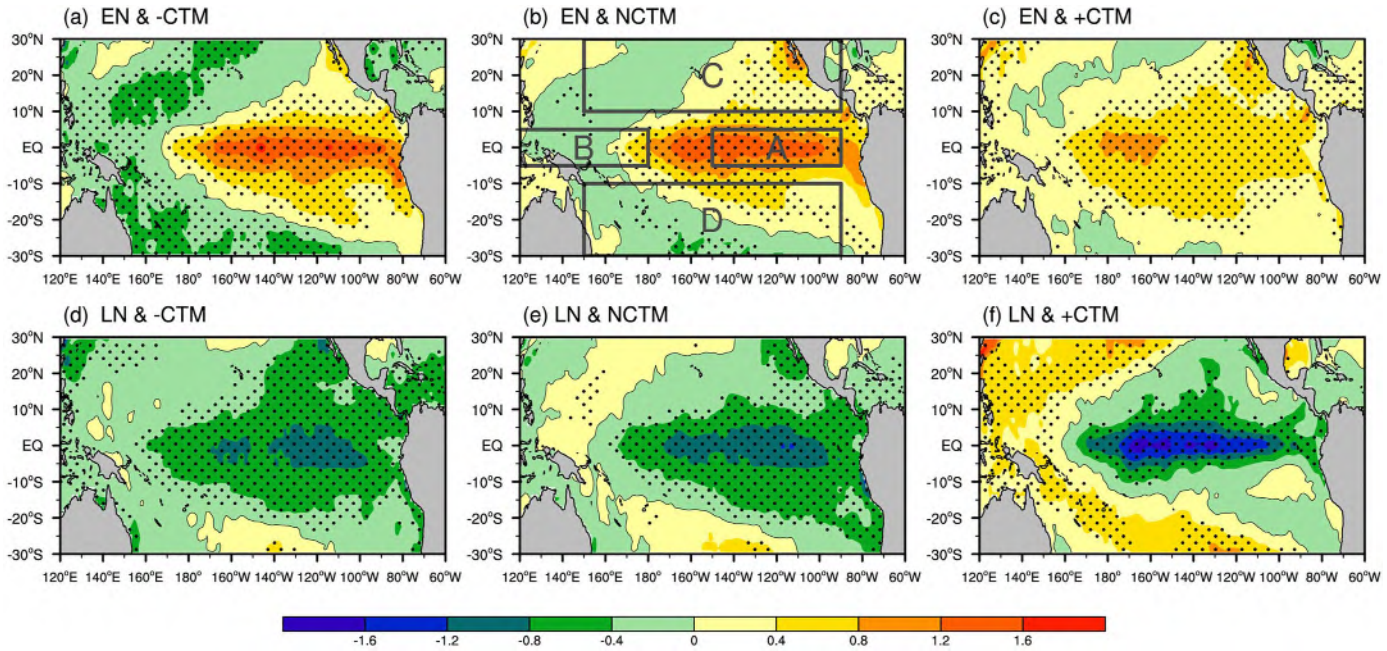

Figure 6. Composites of the SSTA (°C) during boreal winter (DJF) for the combinations of the three CTM phases and El Niño or La Niña. El Niño (EN) or La Niña (LN) is defined such that the winter NPC1 is greater than 0.5 or smaller than −0.5 SD. The +CTM or −CTM is defined such that the winter NPC2 is greater than 0.5 or smaller than −0.5 SD. Others are defined as the normal CTM (NCTM). In all plots, stippled regions indicate statistical significance at the 99% confidence level, and the thin black contours denote zero lines. The four boxes are A (5°S–5°N, 150°W–90°W), B (5°S–5°N, 120°E–180°E), C (10°N–30°N, 150°E–90°W), and D (10°S–30°S, 150°E–90°W).

3.3. Impacts of the CTM on La Niña Diversity

The CTM also has an impact on La Niña diversity. Table 2 shows that the La Niña & −CTM and La Niña & NCTM classes occur frequently before 1980, and the La Niña & +CTM class occurs most frequently after 1980. Figures 6d–6f show composite distributions of these three La Niña classes. Note that the La Niña & NCTM and La Niña & +CTM classes exhibit the conventional La Niña horseshoe pattern. However, the La Niña & −CTM class has cold SSTA over almost the whole tropical Pacific. Moving from the La Niña & −CTM to La Niña & +CTM class, there is cooling of the eastern equatorial SSTA and warming of the SSTA outside the eastern equatorial Pacific (Figure 7d). The zonal and meridional widths gradually decrease from the La Niña & −CTM to La Niña & +CTM class (Figure 7e). In addition, the longitude of the La Niña & +CTM center is approximately located in the central equatorial Pacific, and the centers of the other classes are located in the eastern equatorial Pacific (Figure 7f).

Similar to three El Niño classes, we also provide an alternative explanation to the impact of the CTM on La Niña spatial pattern. If a negative CTM is superposed on La Niña, its warm SSTA in the eastern equatorial Pacific may weaken the eastern equatorial SSTA of La Niña (Figure 7d). The negative CTM's cold SSTA may cool the La Niña SSTA in the western equatorial and off-equatorial Pacific (Figure 7d), which is favorable for the wider zonal and meridional widths of La Niña (Figure 7e). Conversely, when a positive CTM is superposed on La Niña, the additional cold SSTA in the eastern equatorial Pacific may increase the equatorial cooling SSTA of La Niña (Figure 7d). Meanwhile, the positive CTM's warming SSTA outside the eastern equatorial Pacific could warm the western equatorial and off-equatorial SSTA of La Niña (Figure 7d), which is favorable for the narrower zonal and meridional widths of La Niña (Figure 7e). In addition, the impact of a normal CTM on La Niña is again small, and all the spatial characteristics of the La Niña & NCTM class remain in a normal or intermediate state.

3.4. Impacts of the CTM on the Bjerknes Feedback Strength of ENSO Classes

It is well known that the Bjerknes feedback (BF) makes a dominant contribution to ENSO evolution (e.g., Bjerknes, 1969; Capotondi, 2013; Fedorov & Philander, 2001; Jin, 1997a, 1997b; Karnauskas, 2013). Recently, Ren and Jin (2013) emphasized that the BF also plays a dominant role in contributing to the growth of CP-El Niño. Since the CTM can well represent the long-term trend of the tropical Pacific under global warming (Li

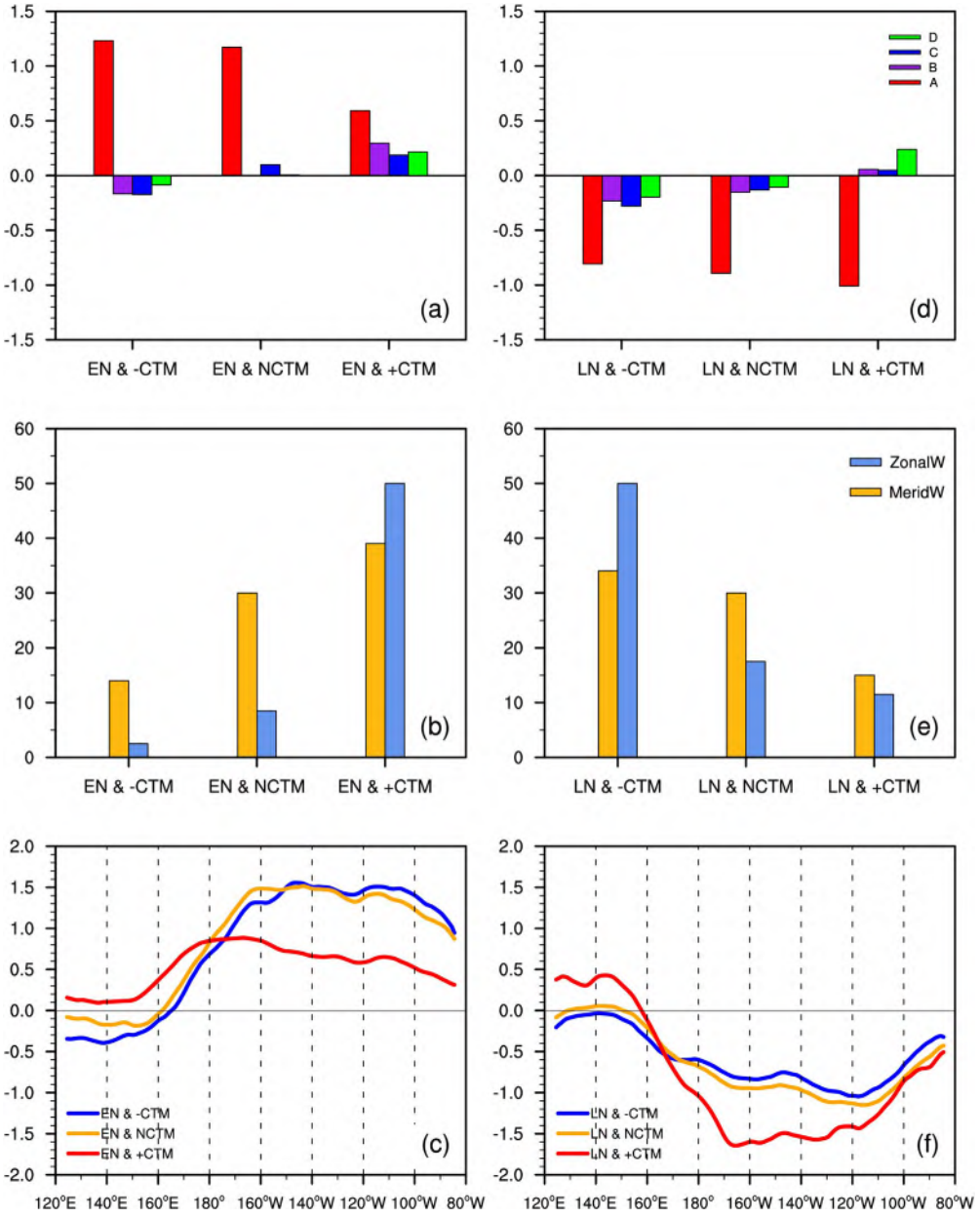

Figure 7. Characteristics of spatial pattern for the three El Niño and La Niña classes. (a) SSTA averages in four areas (°C), (b) zonal (cornflower blue bar) and meridional (orange bar) widths (°), and (c) 10 point running average (°C) from 5°S to 5°N along the Pacific equator for the three El Niño classes. (d)–(f) As in Figures 7a–7c, but for three La Niña classes. The four areas are A (5°S–5°N, 150°W–90°W), B (5°S–5°N, 120°E–180°E), C (10°N–30°N, 150°E–90°W), and D (10°S–30°S, 150°E–90°W). To allow convenient comparison, 100° and 20° are, respectively, subtracted from the zonal widths and meridional widths in Figures 7b and 7e.

et al., 2015; Zhang et al., 2010), the BF of ENSO is expected to be modified by the CTM. Meanwhile, Jin et al. (2006) have pointed out that the BF represents the dynamic coupling of zonal wind stress, SST, and thermocline depth. To reveal the impacts of the CTM on the BF, we first investigate the evolution of these three representative variables associated with ENSO growth. Note that SSH is used as a proxy of thermocline depth in our study, because of data availability.

Figure 8 shows a longitude-time section of the composite zonal wind stress, SSTA, and SSHA patterns for three El Niño classes. Their common feature is a peak phase in DJF. As shown in Figures 8a–8c, the three representative variables (zonal wind stress anomaly, SSTA, and SSHA) of the El Niño & −CTM class is

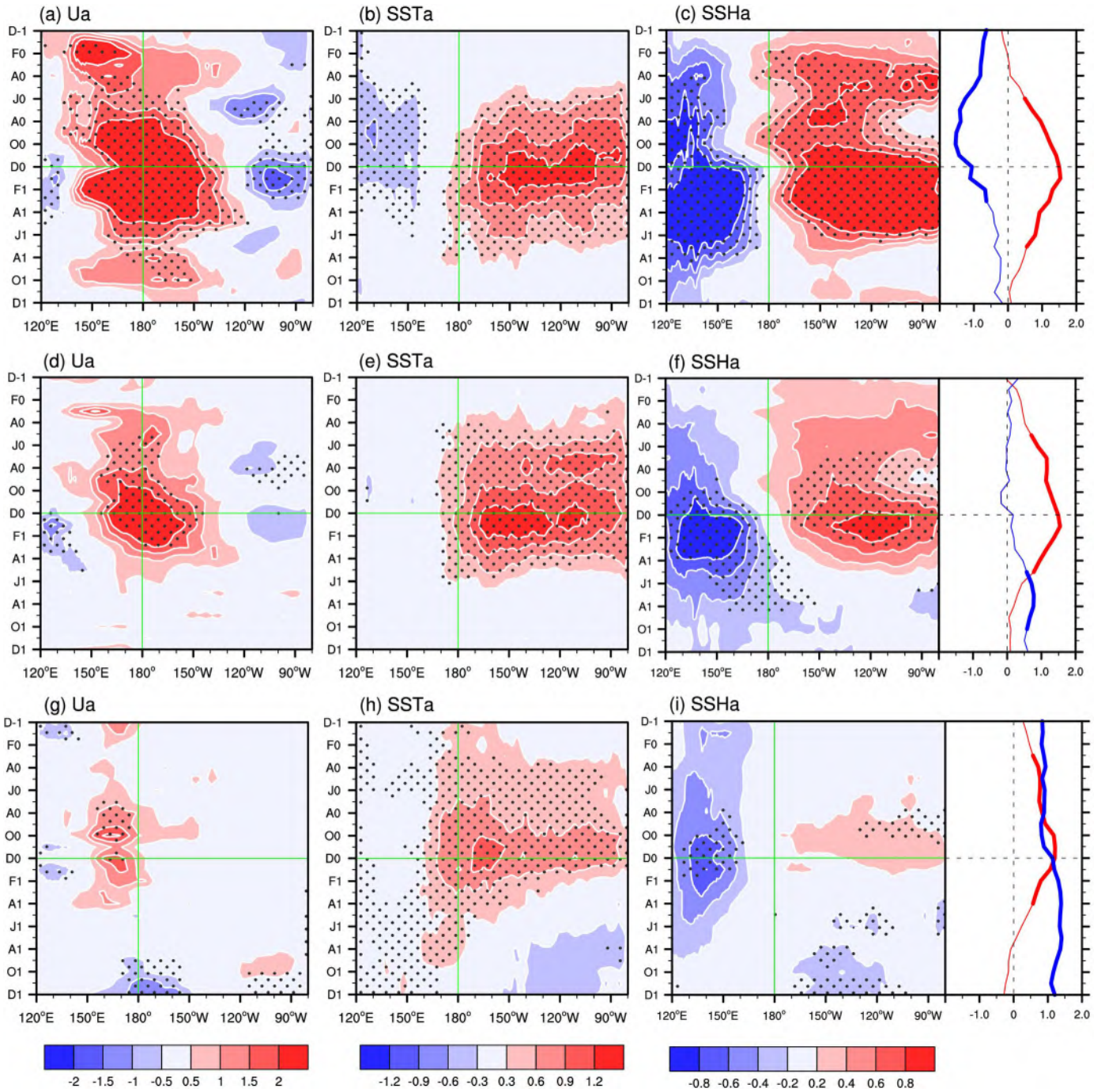

Figure 8. (a)–(c) Longitude-time section of the composite zonal wind stress (0.01 N m^{-2}), SSTA (°C), and SSHA (dm) at the equatorial Pacific (averaged from 5°S to 5°N) for the El Niño & −CTM class. (d)–(f) and (g)–(i) As in Figures 8a–8c, but for the El Niño & NCTM and El Niño & +CTM classes, respectively. The ordinate presents a 25-month period from December of year −1 to December of year 1. Stippled regions indicate statistical significance at the 95% confidence level. Red and blue lines denote the composite NPC1 and NPC2, respectively; thicker lines indicate the 95% confidence level.

strongest among these three El Niño classes. For the El Niño & +CTM class, the warm SSTA develops earlier in the central equatorial Pacific (Figure 8h), and the intensity of three representative variables is weaker than that of the other two El Niño classes (Figure 8). In addition, the three representative variables of El Niño & NCTM class is intermediate and its corresponding intensity of the CTM is almost zero during the developing period (Figures 8d–8f).

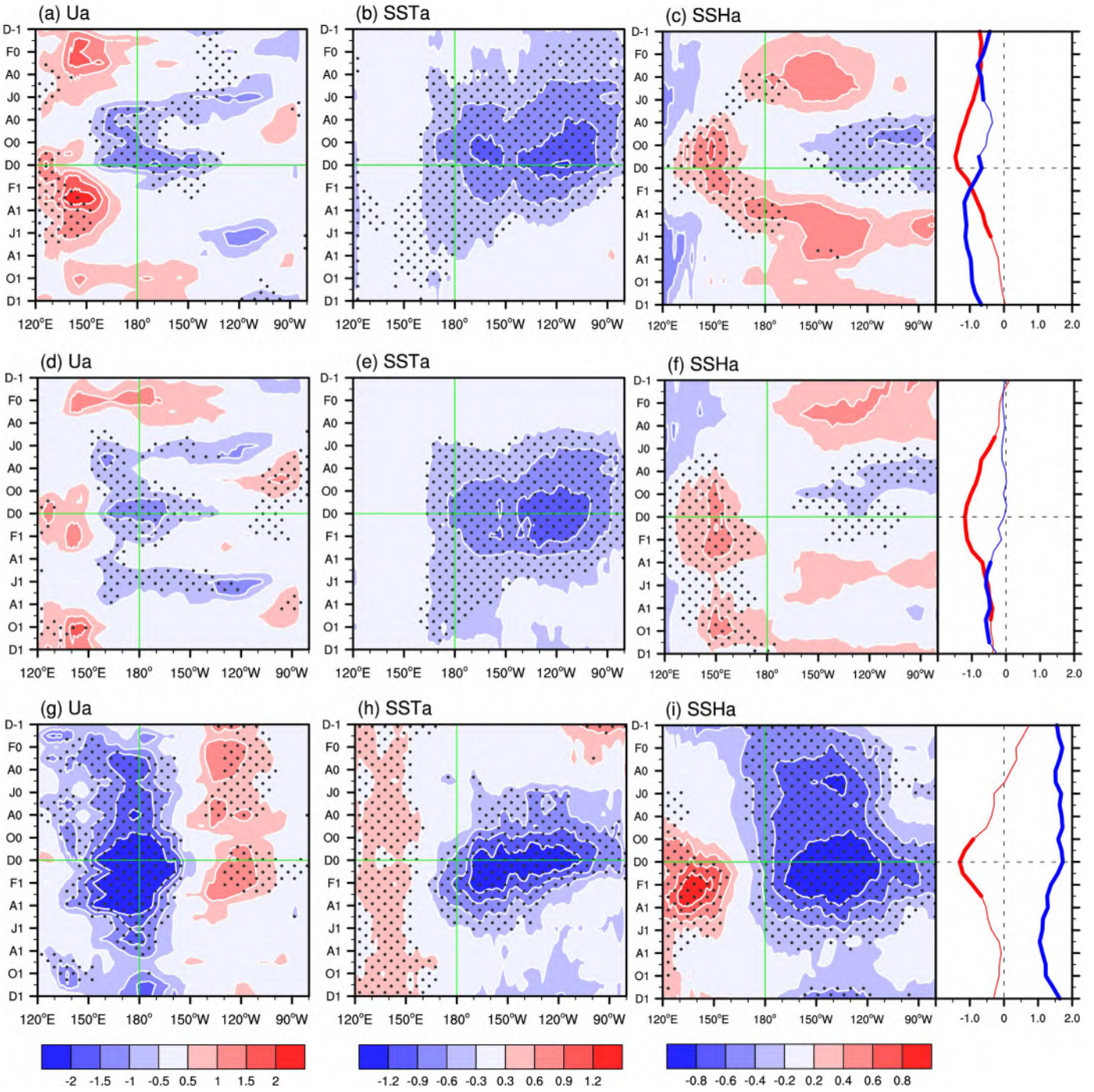

Figure 9. As in Figure 8, but for (a)–(c) La Niña & −CTM, (d)–(f) La Niña & NCTM, and (g)–(i) La Niña & +CTM classes, respectively.

In La Niña & −CTM class (Figures 9a–9c), the intensity of three representative variables is slightly stronger than that of the La Niña & NCTM class during developing period (not shown). This is because the corresponding La Niña intensity of the La Niña & −CTM class is slightly stronger than that of the La Niña & NCTM class (red lines in Figures 9c and 9f). In addition, although the CTM of the La Niña & −CTM class is negative, it is not significant during developing period (blue line, Figure 9c). For the La Niña & +CTM class, its corresponding intensity of three representative variables is strongest among these three La Niña classes (Figures 9g–9i).

It is interesting to note that the positive or negative CTM is always significant during the developing phase of ENSO (blue line, Figures 8c, 8i, and 9i), except for the La Niña & −CTM class (blue line, Figure 9c). This is suggested that the CTM could persistently impact on the ENSO growth, and thus the CTM may play an important role in the BF of ENSO. As seen in Figures 8 and 9, July–November of year 0 is the period of primary growth for all three El Niño and La Niña classes. To more clearly reveal the impacts of the CTM on the BF of ENSO, in the following we also quantitatively examine the BF intensity of different ENSO classes during developing phase (July–November of year 0). Following previous studies (e.g., Chen et al., 2015; Liu et al., 2011), the ENSO growth rate (σ) associated with the BF is shown as follows:

$$\sigma = \frac{\bar{w}}{H} R(\tau'_x, T') R(D', \tau'_x) R(T'_e, D')$$

where primes indicate the monthly anomaly. The variables $\bar{w}$, H, τ_x, T, D, and T_e indicate mean vertical current, climatological mixed layer depth in the eastern equatorial Pacific (H = 50 m), zonal wind stress, SST, thermocline depth, and subsurface temperature, respectively. Note that the analysis formula here with respect to the BF is in a way similar to that applied in the Bjerknes coupled stability index (e.g., Chen et al., 2016; Jin et al., 2006; Kim & Jin, 2011a, 2011b; Marathe et al., 2015). Except for the area of τ_x (central equatorial Pacific [CEP]: 2°S–2°N, 150°E–160°W), the calculated area of all terms is located in the eastern equatorial Pacific (EEP: 2°S–2°N, 160°W–90°W). This equation depicts that the growth rate associated with BF involves three feedback processes. Namely, the first feedback $R(\tau'_x, T')$ represents the atmospheric response of zonal wind stress in the CEP to a unit SSTA forcing in the EEP, the second feedback $R(D', \tau'_x)$ represents the response of ocean thermocline depth in the EEP to a unit zonal wind stress forcing in the CEP, and the third feedback $R(T'_e, D')$ represents the response of the subsurface temperature to a unit thermocline depth change in the EEP (e.g., Chen et al., 2015). In this study, it is noted that $R(\tau'_x, T')$, $R(D', \tau'_x)$, and $R(T'_e, D')$ are all slope values of dynamic coupling strength during ENSO developing phase, and that SSH is used as a proxy of thermocline depth, because of data availability.

As shown in Figure 10a, the values of $R(\tau'_x, T')$ and $R(D', \tau'_x)$ gradually weaken from the El Niño & −CTM to El Niño & +CTM class. Namely, the response of zonal wind stress to SST and the response of ocean thermocline to zonal wind stress of El Niño & +CTM class is weakest, and that of El Niño & −CTM class is strongest, as well as that of El Niño & NCTM class is normal (Figure 10a). The change of BF intensity (σ) among three El Niño classes is consistent with that of $R(\tau'_x, T')$ and $R(D', \tau'_x)$, although it is inconsistent with that of $R(T'_e, D')$. This means that the BF intensity is controlled by the response of zonal wind stress to SST and the response of ocean thermocline to zonal wind stress.

It is similar to the results of Marathe et al. (2015), which shows the response of zonal wind stress to SSTA plays a major contributor to BF. Meanwhile, Zhang et al. (2010) and Li et al. (2015) emphasized that the CTM corresponds the long-term cooling trend of sea temperature in the eastern equatorial Pacific under global warming (Figures 1 and 4a). In other words, a positive CTM can provide a cooling background of the eastern equatorial Pacific during ENSO evolution, with conditions reversed for a negative CTM. Therefore, it is suggested that a positive CTM could suppress the response of zonal wind stress to SST and the response of ocean thermocline to zonal wind stress, and thus suppress the BF intensity of El Niño & +CTM class in the eastern equatorial Pacific. This can prevent the SSTA growth of El Niño & +CTM class in the eastern equatorial Pacific, and thus induce a westward shift of SSTA center of El Niño & +CTM class (Figure 6c). These results are consistent with Karnauskas (2013). Similarly, a negative CTM is likely to strengthen the BF intensity of El Niño & −CTM class through modifying these two important responses. In addition, El Niño & NCTM class has the intermediate BF intensity (Figure 10a) and the impact of the CTM on its BF can be ignored, because its corresponding CTM intensity is almost zero during El Niño evolution (Figure 8f).

Figure 10b depicts that the change of $R(\tau'_x, T')$ and $R(D', \tau'_x)$ among three La Niña classes is consistent with that of BF intensity. Also, it shows that the BF intensity of La Niña & +CTM class is strongest, that of La Niña & NCTM class is weakest, and that of La Niña & −CTM class is normal. Considering the cooling eastern equatorial Pacific associated with the positive CTM, it is suggested that a positive CTM may strengthen the response of zonal wind stress to SST and the response of ocean thermocline to zonal wind stress, and thus strengthen the BF intensity of La Niña & +CTM class. In addition, the impact of the CTM on BF intensity of La Niña & NCTM class can be ignored, because the corresponding CTM intensity is almost zero during La Niña evolution (Figure 9f). Since a negative CTM corresponds to the warming background in the eastern

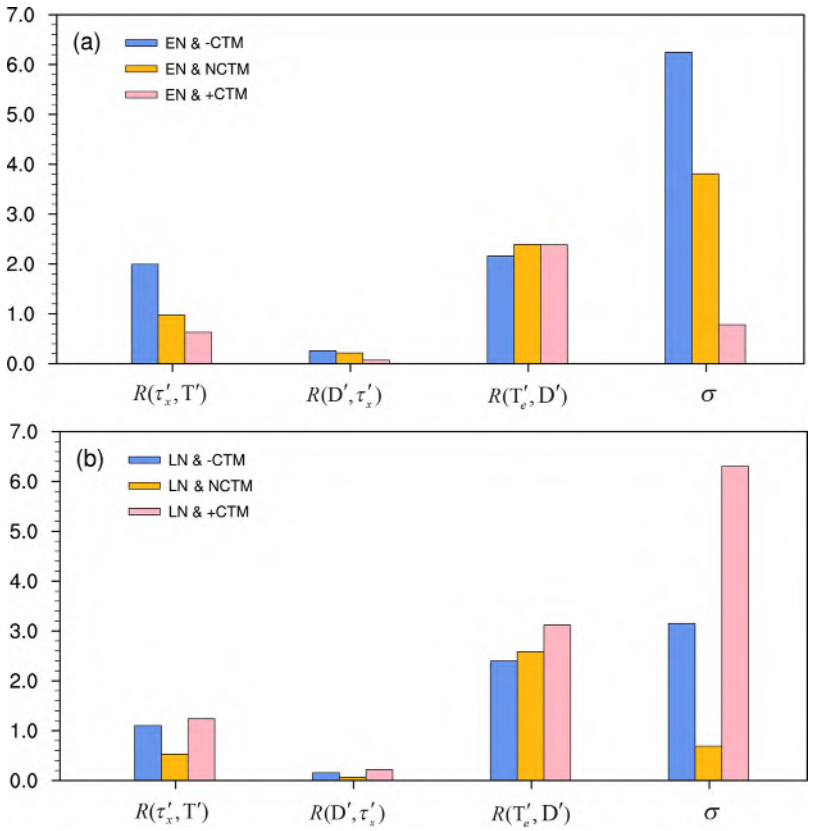

Figure 10. (a) The histogram shows the slope values associated with the BF intensity during developing phase (from July–November) for El Niño & −CTM (cornflower blue), El Niño & NCTM (orange), and El Niño & +CTM (pink) classes. $R(\tau'_x, T')$ represents the zonal wind stress-SST for air-sea coupling coefficient (10^{-2} Nm^{-2} $°C^{-1}$). $R(D', \tau'_x)$ and $R(T'_e, D')$ represent the thermocline-wind (10^2 dm $N^{-1}m^2$) and thermocline-subsurface temperature (°C dm^{-1}) coupling coefficients, respectively. σ is the growth rate associated with the BF intensity (yr^{-1}). (b) The histogram is same as Figure 10a, but for La Niña & −CTM (cornflower blue), La Niña & NCTM (orange), and La Niña & +CTM (pink) classes. All coupling coefficients are significant above 90% confidence level, except for $R(D', \tau'_x)$ of La Niña & NCTM in histogram (b), which exceeds the 88% confidence level.

equatorial Pacific, the BF intensity of La Niña & −CTM class is expected to be weakened in comparison with that of La Niña & NCTM class. However, it is interesting to note that the BF intensity of La Niña & −CTM class is stronger than that of La Niña & NCTM class (Figure 10b). Maybe, this is caused by two reasons. First, although a negative CTM is superposed on La Niña, the CTM intensity in La Niña & −CTM class is not significant during its developing period (blue line, Figure 9c), and thus the impact of the negative CTM on La Niña BF intensity is very weak. Second, the La Niña intensity of La Niña & −CTM class (red line in Figure 9c) is slightly stronger than that of La Niña & NCTM class (red line in Figure 9f) during developing period. These two reasons may cause the stronger BF intensity of La Niña & −CTM class in comparison with that of La Niña & NCTM class.

4. Discussion and Conclusions

This study first investigates the long-term trend of the oceanic temperature anomaly averaged from surface to subsurface (T') in the equatorial Pacific under global warming. Although the two data sets exhibit some differences in the 7 year Gaussian low-pass filtered T' (Figure 2), they all show a long-term cooling trend in the eastern equatorial Pacific (Figure 4a). In addition, both data sets after filtering ENSO signal clearly display a change of the term $\partial T'/\partial z$ from a positive to a negative state in the eastern equatorial Pacific (Figure 3). Based on the ocean dynamical feedback associated with the CTM (Li et al., 2015), this decreasing term $\partial T'/\partial z$ accompanied by the mean upwelling could induce the cooling vertical advection, which makes a contribution to the cooling ocean temperature in the eastern equatorial Pacific. These results suggest that the

Table 3
Characteristics of the Three El Niño and La Niña Classes

	Meridional width	Zonal width	Outside of EP	Eastern Pacific (EP)	Central location
El Niño & −CTM	Narrower	Narrower	Cooler	Warmer	East
El Niño & NCTM	Norm	Norm	Norm	Norm	East
El Niño & +CTM	Wider	Wider	Warmer	Cooler	West
La Niña & −CTM	Wider	Wider	Cooler	Warmer	East
La Niña & NCTM	Norm	Norm	Norm	Norm	East
La Niña & +CTM	Narrower	Narrower	Warmer	Cooler	West

decreasing term $\partial T'/\partial z$ contributes to the long-term cooling trend in the eastern equatorial Pacific through the ocean dynamical feedback associated with the CTM under global warming. Therefore, these results reconfirm that the ocean dynamical feedback associated with the CTM is responsible for the long-term cooling trend of the eastern equatorial Pacific under global warming.

Our results also demonstrate that the long-term trend in the CTM contributes to ENSO diversity in its spatial pattern. Before 1940, the El Niño & −CTM class occurs most frequently (14 events) among three El Niño classes (Table 1). After 1940, the El Niño & −CTM class includes just two events, but the El Niño & +CTM class becomes most frequent (14 events), especially for the post-1980 period (Table 1). During the post-1980 period, the La Niña & +CTM class is the most frequent (seven events) among three La Niña classes (Table 2). However, there are no La Niña & +CTM events before 1980 (Table 2). In contrast, the La Niña & −CTM class consists of 19 events before 1980 (Table 2). These distributions of ENSO classes are closely related to the long-term trend of the CTM under global warming. In addition, although some studies suggested that the third EOF mode (EOF3) of the tropical Pacific SSTA can well represent the Modoki mode (e.g., L'Heureux et al., 2013a), the EOF3 mode only accounts for 64% of the Modoki variance. It is also noted that the composite SSTA for the combinations of the EOF3 mode and ENSO (not shown) is different from the composite SSTA for the combinations of the CTM and ENSO (Figure 6). This is suggested that the impact of the CTM on ENSO is different from that of the EOF3 mode.

It is also found that the CTM can modify the spatial properties of ENSO in its zonal and meridional structure as well as center location (more details in Table 3). This result could be further proved through the composites of the SSTA without the CTM signal during boreal winter (DJF) for the six ENSO classes (same as Figure 6), which all shows the typical ENSO horseshoe pattern in the tropical Pacific. Meanwhile, the CTM provides a background state for ENSO evolution, and thus modifies the BF intensity of ENSO during developing period. A positive CTM weakens (strengthens) the BF intensity of El Niño (La Niña) in the eastern equatorial Pacific, while a negative CTM strengthens the BF intensity of El Niño in the eastern equatorial Pacific. Interestingly, when a positive CTM is superposed on El Niño, the center location of El Niño & +CTM class is similar to that of CP-El Niño. It is because the positive CTM can weaken the BF intensity of El Niño and prevent its SSTA growth in the eastern equatorial Pacific, and thus induce a westward shift of SSTA center of El Niño (Figure 6c). Considering the long-term trend of the CTM (Figure 1), it is suggested that the CTM contributes to more frequent occurrence of CP-El Niño under global warming. Furthermore, the corresponding negative CTM is weak and not significant during the developing phase of La Niña, and therefore the impacts of negative CTM on the BF intensity of La Niña is also weak. However, the CTM intensity of La Niña & −CTM class starts to become significant from November (year 0) (Figure 9c), and thus the negative CTM rapidly weakens the SSTA in the eastern equatorial Pacific (Figure 9b).

In addition, the center of action associated with the La Niña & +CTM class is shifted westward into the central equatorial Pacific, which is consistent with Zhang et al. (2015). Their Figure 1 also shows that CP-La Niña is characterized by a SSTA cooling center confined to the central equatorial Pacific. Note that the center of the La Niña & +CTM class cannot be explained by the alternative explanation mentioned above. Maybe the nonlinear dynamic heating associated with the ENSO growth (e.g., Jin et al., 2003) contributes to the center of the La Niña & +CTM class. Nevertheless, the alternative explanation can explain the change of equatorial and off-equatorial SSTA and the zonal and meridional structure in all ENSO classes, as well as the center location of the El Niño & +CTM class.

It is suggested that the CTM could explain a part of ENSO diversity. Zhang et al. (2015) have pointed out that the fundamental dynamics of generation associated with ENSO diversity are not well understood at present. It is because there are many factors influencing ENSO diversity, for example, global warming (e.g., Ashok et al., 2007; Collins et al., 2010; Duan et al., 2014; Yeh et al., 2009), westerly wind bursts (WWBs) (e.g., Chen et al., 2015; Fedorov et al., 2015; Hu et al., 2014; Lian et al., 2014; Lopez & Kirtman, 2013), Pacific decadal oscillation (PDO) (e.g., Choi et al., 2011, 2012; Chung & Li, 2013; Xiang et al., 2013), and NPO (e.g., Ding et al., 2015a, 2015b, 2015c; Yeh et al., 2015; Yu & Kim, 2011). The interaction of these different factors, their contributions to ENSO diversity, and their relationship with the CTM are fundamental topics, requiring further investigation. Particularly for the PDO (e.g., Mantua & Hare, 2002; Mantua et al., 1997; Newman et al., 2016; Zhang et al., 1997), it is independent from the CTM, because of their completely different spatial and temporal characteristics, as well as different physical mechanism. To further clarify the independence between the CTM and PDO, we first remove the PDO signal and then perform EOF analysis over the tropical Pacific. The obtained CTM (not shown) is essentially same as raw CTM (Figure 1), because their corresponding spatial and temporal correlation coefficients are approximately 1.0. Meanwhile, the impacts of the CTM on ENSO are also different from that of the PDO. It is because the CTM mainly represents the impact of ocean dynamical process on ENSO under global warming. But the PDO mainly represents the impact of internal decadal variability on ENSO.

Although the more frequent occurrence of CP-El Niño can produce a warming in the central equatorial Pacific and a cooling in the eastern equatorial Pacific, its contribution to the CTM may not be dominant. When we remove the CP-El Niño signal and then perform EOF analysis over the tropical Pacific, the obtained CTM (not shown) is essentially same as raw CTM (Figure 1). However, the interaction between the background mean state and ENSO under global warming is still unclear (e.g., Capotondi et al., 2015). For example, McPhaden et al. (2011) argued that the more frequent occurrence of CP-El Niño events can modulate the tropical Pacific mean state. It is noted that our study just provides an alternative explanation to the impacts of the CTM on ENSO diversity and briefly discusses the impacts of the CTM on BF intensity of ENSO. In the future work, we intend to carry out further research into the specific dynamics and thermodynamic processes associated with the impacts of the CTM on ENSO diversity, and this should help to more clearly understand the interaction between the background mean state and ENSO under global warming.

Acknowledgments
We acknowledge the helpful suggestions and comments of three anonymous reviewers. This work was jointly supported by the National Natural Science Foundation of China (NSFC) Project (41530424, 41375110), SOA International Cooperation Program on Global Change and Air-Sea Interactions (GASI-IPOVAI-03), and China Meteorological Administration Special Public Welfare Research Fund (GYHY201506013), and National Key R&D Program of China (2016YFA0601801). The HadISST1 was obtained from the Met Office Hadley Centre and can be downloaded from http://www.metoffice.gov.uk/hadobs/hadisst/data/download.html. The SODA data set was obtained from the National Center for Atmospheric Research (NCAR) and can be downloaded from http://dsrs.atmos.umd.edu/DATA/soda_2.2.4/. The ORAS4 data set was obtained from the CliSAP Integrated Climate Data Center and was downloaded from ftp://ftp.icdc.zmaw.de/EASYInit/ORA-S4/.

References

Ashok, K., Behera, S. K., Rao, S. A., Weng, H. Y., & Yamagata, T. (2007). El Niño Modoki and its possible teleconnection. *Journal of Geophysical Research*, *112*, C11007. https://doi.org/10.1029/2006JC003798

Balmaseda, M. A., Mogensen, K., & Weaver, A. T. (2013a). Evaluation of the ECMWF ocean reanalysis system ORAS4. *Quarterly Journal of the Royal Meteorological Society*, *139*, 1132–1161. https://doi.org/10.1002/qj.2063

Balmaseda, M. A., Trenberth, K. E., & Kallen, E. (2013b). Distinctive climate signals in reanalysis of global ocean heat content. *Geophysical Research Letters*, *40*, 1754–1759. https://doi.org/10.1002/grl.50382

Battisti, D. S., & Hirst, A. C. (1989). Interannual variability in a tropical atmosphere-ocean model: Influence of the basic state, ocean geometry and nonlinearity. *Journal of the Atmospheric Sciences*, *46*, 1687–1712. https://doi.org/10.1175/1520-0469(1989)046<1687:IVIATA>2.0.CO;2

Bjerknes, J. (1969). Atmospheric teleconnections from equatorial Pacific. *Monthly Weather Review*, *97*, 163–172. https://doi.org/10.1175/1520-0493(1969)097<0163:ATFTEP>2.3.CO;2

Bond, N. A., Overland, J. E., Spillane, M., & Stabeno, P. (2003). Recent shifts in the state of the North Pacific. *Geophysical Research Letters*, *30*(23), 2183. https://doi.org/10.1029/2003GL018597

Cane, M. A., Clement, A. C., Kaplan, A., Kushnir, Y., Pozdnyakov, D., Seager, R., . . . Murtugudde, R. (1997). Twentieth-century sea surface temperature trends. *Science*, *275*(5302), 957–960. https://doi.org/10.1126/science.275.5302.957

Capotondi, A. (2013). ENSO diversity in the NCAR CCSM4 climate model. *Journal of Geophysical Research: Oceans*, *118*, 4755–4770. https://doi.org/10.1002/jgrc.20335

Capotondi, A., Wittenberg, A. T., Newman, M., Lorenzo, E. D., Yu, J. Y., Braconnot, P., . . . Yeh, S. W. (2015). Understanding ENSO diversity. *Bulletin of the American Meteorological Society*, *96*, 921–938. https://doi.org/10.1175/BAMS-D-13-00117.1

Carton, J. A., & Giese, B. S. (2008). A reanalysis of ocean climate using simple ocean data assimilation (SODA). *Monthly Weather Review*, *136*(8), 2999–3017. https://doi.org/10.1175/2007MWR1978.1

Chen, D. K., Lian, T., Fu, C. B., Cane, M. A., Tang, Y. M., Murtugudde, R., . . . Zhou, L. (2015). Strong influence of westerly wind bursts on El Niño diversity. *Nature Geoscience*, *8*, 339–345. https://doi.org/10.1038/ngeo2399

Chen, L., Li, T., & Yu, Y. (2015). Causes of strengthening and weakening of ENSO amplitude under global warming in four CMIP5 models. *Journal of Climate*, *28*, 3250–3274. https://doi.org/10.1175/JCLI-D-14–00439.1

Chen, L., Yu, Y., & Zheng, W. (2016). Improved ENSO simulation from climate system model FGOALS-g1. 0 to FGOALS-g2. *Climate Dynamics*, *47*, 2617–2634. https://doi.org/10.1007/s00382-016-2988-8

Choi, J., An, S. I., Kug, J. S., & Yeh, S. W. (2011). The role of mean state on changes in El Niño's flavor. *Climate Dynamics*, *37*(5–6), 1205–1215. https://doi.org/10.1007/s00382-010-0912-1

Choi, J., An, S. I., & Yeh, S. W. (2012). Decadal amplitude modulation of two types of ENSO and its relationship with the mean state. *Climate Dynamics*, *38*, 2631–2644. https://doi.org/10.1007/s00382-011-1186-y

Chung, P. H., & Li, T. (2013). Interdecadal relationship between the mean state and El Niño types. *Journal of Climate*, *26*, 361–379. https://doi.org/10.1175/JCLI-D-12–00106.1

Clement, A. C., Seager, R., Cane, M. A., & Zebiak, S. E. (1996). An ocean dynamical thermostat. *Journal of Climate*, *9*(9), 2190–2196. https://doi.org/10.1175/1520-0442(1996)009<2190:AODT>2.0.CO;2

Collins, M., An, S. I., Cai, W. J., Ganachaud, A., Guilyardi, E., Jin, F. F., . . . Wittenberg, A. (2010). The impact of global warming on the tropical Pacific Ocean and El Niño. *Nature Geoscience*, *3*(6), 391–397. https://doi.org/10.1038/ngeo868

Compo, G. P., & Sardeshmukh, P. D. (2010). Removing ENSO–related variations from the climate record. *Journal of Climate*, *23*(8), 1957–1978. https://doi.org/10.1175/2009JCLI2735.1

DiNezio, P. N., Clement, A. C., Vecchi, G. A., Soden, B. J., & Kirtman, B. P. (2009). Climate response of the equatorial Pacific to global warming. *Journal of Climate*, *22*(18), 4873–4892. https://doi.org/10.1175/2009JCLI2982.1

Ding, R., Li, J., & Tseng, Y.-H. (2015a). The impact of South Pacific extratropical forcing on ENSO and comparisons with the North Pacific. *Climate Dynamics*, *44*, 2017–2034. https://doi.org/10.1007/s00382-014-2303-5

Ding, R., Li, J., Tseng, Y.-H., & Ruan, C. (2015b). Influence of the North Pacific Victoria mode on the Pacific ITCZ summer precipitation. *Journal of Geophysical Research: Atmospheres*, *120*, 964–979. https://doi.org/10.1002/2014JD022364

Ding, R., Li, J., Tseng, Y.-H., Sun, C., & Guo, Y. (2015c). The Victoria mode in the North Pacific linking extratropical sea level pressure variations to ENSO. *Journal of Geophysical Research: Atmospheres*, *120*, 27–45. https://doi.org/10.1002/2014JD022221

Drenkard, E. J., & Karnauskas, K. B. (2014). Strengthening of the Pacific equatorial undercurrent in the SODA reanalysis: Mechanisms, ocean dynamics, and implications. *Journal of Climate*, *27*(6), 2405–2416. https://doi.org/10.1175/JCLI-D-13-00359.1

Duan, W. S., Tian, B., & Xu, H. (2014). Simulations of two types of El Niño events by an optimal forcing vector approach. *Climate Dynamics*, *43*(5–6), 1677–1692. https://doi.org/10.1007/s00382-013-1993-4

Fedorov, A. V., Hu, S., Lengaigne, M., & Guilyardi, E. (2015). The impact of westerly wind bursts and ocean initial state on the development, and diversity of El Niño events. *Climate Dynamics*, *44*, 1381–1401. https://doi.org/10.1007/s00382-014-2126-4

Fedorov, A. V., & Philander, S. G. (2001). A stability analysis of tropical ocean-atmosphere interactions: Bridging measurements and theory for El Niño. *Journal of Climate*, *14*, 3086–3101. https://doi.org/10.1175/1520-0442(2001)014<3086:ASAOTO>2.0.CO;2

Feng, J., & Li, J. (2011). Influence of El Niño Modoki on spring rainfall over south China. *Journal of Geophysical Research*, *116*, D13102. https://doi.org/10.1029/2010JD015160

Feng, J., & Li, J. (2013). Contrasting impacts of two types of ENSO on the boreal spring Hadley circulation. *Journal of Climate*, *26*, 4773–4789. https://doi.org/10.1175/JCLI-D-12–00298.1

Feng, J., Li, J., Zheng, F., Xie, F., & Sun, C. (2016a). Contrasting impacts of developing phases of two types of El Niño on Southern China rainfall. *Journal of the Meteorological Society of Japan: Series II*, *94*, 359–370. https://doi.org/10.2151/jmsj. 2016-019

Feng, J., Li, J, Zhu, J., & Liao, H. (2016b). Influences of El Niño Modoki event 1994/1995 on aerosol concentrations over southern China. *Journal of Geophysical Research: Atmospheres*, *121*, 1637–1651. https://doi.org/10.1002/2015JD023659

Feng, J., Wu, Z., & Zou, X. (2014). Sea surface temperature anomalies off Baja California: A possible precursor of ENSO. *Journal of the Atmospheric Sciences*, *71*, 1529–1537. https://doi.org/10.1175/JAS-D-13–0397.1

Funk, C. C., & Hoell, A. (2015). The leading mode of observed and CMIP5 ENSO-residual sea surface temperatures and associated changes in Indo-Pacific climate. *Journal of Climate*, *28*, 4309–4329. https://doi.org/10.1175/JCLI-D-14-00334.1

Garfinkel, C. I., Hurwitz, M. M., Oman, L. D., & Waugh, D. W. (2013). Contrasting effects of Central Pacific and Eastern Pacific El Niño on stratospheric water vapor. *Geophysical Research Letters*, *40*, 4115–4120. https://doi.org/10.1002/grl.50677

Hu, S., Fedorov, A. V., Lengaigne, M., & Guilyardi, E. (2014). The impact of westerly wind bursts on the diversity and predictability of El Niño events: An ocean energetics perspective. *Geophysical Research Letters*, *41*, 4654–4663. https://doi.org/10.1002/2014GL059573

Jin, F. F. (1997a). An equatorial ocean recharge paradigm for ENSO. Part 1: Conceptual model. *Journal of the Atmospheric Sciences*, *54*, 811–829. https://doi.org/10.1175/1520-0469(1997)054<0811:AEORPF>2.0.CO;2

Jin, F. F. (1997b). An equatorial ocean recharge paradigm for ENSO. Part 2: A stripped-down coupled model. *Journal of the Atmospheric Sciences*, *54*, 830–847. https://doi.org/10.1175/1520-0469(1997)054<0830:AEORPF>2.0.CO;2

Jin, F. F., An, S. I., Timmermann, A., & Zhao, J. (2003). Strong El Niño events and nonlinear dynamical heating. *Geophysical Research Letters*, *30*(3), 1120. https://doi.org/10.1029/2002GL016356

Jin, F. F., Kim, S. T., & Bejarano, L. (2006). A coupled-stability index for ENSO. *Geophysical Research Letters*, *33*, L23708. https://doi.org/10.1029/2006GL027221

Kao, H. Y., & Yu, J. Y. (2009). Contrasting eastern–Pacific and central–Pacific types of ENSO. *Journal of Climate*, *22*(3), 615–632. https://doi.org/10.1175/2008JCLI2309.1

Karnauskas, K. B. (2013). Can we distinguish canonical El Niño from Modoki? *Geophysical Research Letters*, *40*, 5246–5251. https://doi.org/10.1002/grl.51007

Karnauskas, K. B., Seager, R., Kaplan, A., Kushnir, Y., & Cane, M. A. (2009). Observed strengthening of the zonal sea surface temperature gradient across the equatorial Pacific Ocean. *Journal of Climate*, *22*(16), 4316–4321. https://doi.org/10.1175/2009JCLI2936.1

Karori, M. A., Li, J. P., & Jin, F. F. (2013). The asymmetric influence of the two types of El Niño and La Niña on summer rainfall over Southeast China. *Journal of Climate*, *26*, 4567–4582. https://doi.org/10.1175/JCLI-D-12–00324.1

Kim, S. T., & Jin, F. F. (2011a). An ENSO stability analysis. Part I: Results from a hybrid coupled model. *Climate Dynamics*, *36*, 1593–1607. https://doi.org/10.1007/s00382-010-0796-0

Kim, S. T., & Jin, F. F. (2011b). An ENSO stability analysis. Part II: Results from the twentieth and twenty-first century simulations of the CMIP3 models. *Climate Dynamics*, *36*, 1609–1627. https://doi.org/10.1007/s00382-010-0872-5

Kug, J. S., Jin, F. F., & An, S. I. (2009). Two types of El Niño events: Cold tongue El Niño and warm pool El Niño. *Journal of Climate*, *22*(6), 1499–1515. https://doi.org/10.1175/2008JCLI2624.1

Larkin, N. K., & Harrison, D. E. (2005). On the definition of El Niño and associated seasonal average US weather anomalies. *Geophysical Research Letters*, *32*, L13705. https://doi.org/10.1029/2005GL022738

Larson, S. M., & Kirtman, B. P. (2014). The Pacific meridional mode as an ENSO precursor and predictor in the North American multimodel ensemble. *Journal of Climate*, *27*, 7018–7032. https://doi.org/10.1175/JCLI-D-14–00055.1

L'Heureux, M. L., Collins, D. C., & Hu, Z. Z. (2013a). Linear trends in sea surface temperature of the tropical Pacific Ocean and implications for the El Niño-Southern oscillation. *Climate Dynamics*, *40*, 1223–1236. https://doi.org/10.1007/s00382-012-1331-2

L'Heureux, M. L., Lee, S., & Lyon, B. (2013b). Recent multidecadal strengthening of the Walker circulation across the tropical Pacific. *Nature Climate Change*, *3*(6), 571–576. https://doi.org/10.1038/nclimate1840

Li, J., Ren, R., Qi, Y., Wang, F., Lu, R., Zhang, P., . . . Yang, Y. (2013). Progress in air-land-sea interactions in Asia and their role in global and Asian climate change (in Chinese). *Chinese Journal of the Atmospheric Sciences*, *37*, 518–538.
Li, Y., Li, J., Zhang, W., Zhao, X., Xie, F., & Zheng, F. (2015). Ocean dynamical processes associated with the tropical Pacific cold tongue mode. *Journal of Geophysical Research: Oceans*, *120*, 6419–6435. https://doi.org/10.1002/2015JC010814
Lian, T., Chen, D., Tang, Y., & Wu, Q. (2014). Effects of westerly wind bursts on El Niño: A new perspective. *Geophysical Research Letters*, *41*, 3522–3527. https://doi.org/10.1002/2014GL059989
Liu, L., Yu, W., & Li, T. (2011). Dynamic and thermodynamic air-sea coupling associated with the Indian ocean dipole diagnosed from 23 WCRP CMIP3 models. *Journal of Climate*, *24*, 4941–4958. https://doi.org/10.1175/2011JCLI4041.1
Lopez, H., & Kirtman, B. P. (2013). Westerly wind bursts and the diversity of ENSO in CCSM3 and CCSM4. *Geophysical Research Letters*, *40*, 4722–4727. https://doi.org/10.1002/grl.50913
Mantua, N. J., & Hare, S. R. (2002). The pacific decadal oscillation. *Journal of Oceanography*, *58*(1), 35–44. https://doi.org/10.1023/A:1015820616384
Mantua, N. J., Hare, S. R., Zhang, Y., Wallace, J. M., & Francis, R. C. (1997). A pacific interdecadal climate oscillation with impacts on Salmon production. *Bulletin of the American Meteorological Society*, *78*, 1069–1079. https://doi.org/10.1175/1520-0477(1997)078<1069:APICOW>2.0.CO;2
Marathe, S., Ashok, K., Swapna, P., & Sabin, T. (2015). Revisiting El Niño Modokis. *Climate Dynamics*, *45*, 3527–3545. https://doi.org/10.1007/s00382-015-2555-8
McPhaden, M. J., Lee, T., & McClurg, D. (2011). El Niño and its relationship to changing background conditions in the tropical Pacific Ocean. *Geophysical Research Letters*, *38*, L15709. https://doi.org/10.1029/2011GL048275
Newman, M., Alexander, M. A., Ault, T. R., Cobb, K. M., Deser, C., Lorenzo, E. D., . . . Smith, C. A. (2016). The pacific decadal oscillation, revisited. *Journal of Climate*, *29*, 4399–4427. https://doi.org/10.1175/JCLI-D-15–0508.1
Picaut, J., Masia, F., & du Penhoat, Y. (1997). An advective-reflective conceptual model for the oscillatory nature of the ENSO. *Science*, *277*, 663–666. https://doi.org/10.1126/science.277.5326.663
Rayner, N. A., Parker, D. E., Horton, E. B., Folland, C. K., Alexander, L. V., Rowell, D. P., . . . Kaplan, A. (2003). Global analyses of sea surface temperature, sea ice, and night marine air temperature since the late nineteenth century. *Journal of Geophysical Research*, *108*(D14), 4407. https://doi.org/10.1029/2002JD002670
Ren, H.-L., & Jin, F.-F. (2011). Niño indices for two types of ENSO. *Geophysical Research Letters*, *38*, L04704. https://doi.org/10.1029/2010GL046031
Ren, H.-L., & Jin, F.-F. (2013). Recharge oscillator mechanisms in two types of ENSO. *Journal of Climate*, *26*, 6506–6523. https://doi.org/10.1175/JCLI-D-12–00601.1
Ren, H.-L., Jin, F.-F., Stuecker, M. F., & Xie, R. (2013). ENSO regime change since the late 1970s as manifested by two types of ENSO. *Journal of the Meteorological Society of Japan: Series II*, *91*, 835–842. http://doi.org/10.2151/jmsj.2013-608
Ren, H.-L., Jin, F.-F., Tian, B., & Scaife, A. A. (2016). Distinct persistence barriers in two types of ENSO. *Geophysical Research Letters*, *43*, 10,973–10,979. https://doi.org/10.1002/2016GL071015
Seager, R., & Murtugudde, R. (1997). Ocean dynamics, thermocline adjustment, and regulation of tropical SST. *Journal of Climate*, *10*(3), 521–534. https://doi.org/10.1175/1520-0442(1997)010<0521:ODTAAR>2.0.CO;2
Solomon, A., & Newman, M. (2012). Reconciling disparate twentieth–century Indo–Pacific ocean temperature trends in the instrumental record. *Nature Climate Change*, *2*(9), 691–699. https://doi.org/10.1038/nclimate1591
Suarez, M. J., & Schopf, P. S. (1988). A delayed action oscillator for ENSO. *Journal of the Atmospheric Sciences*, *45*, 3283–3287. https://doi.org/10.1175/1520-0469(1988)045<3283:ADAOFE>2.0.CO;2
Sun, D. Z., & Liu, Z. Y. (1996). Dynamic ocean-atmosphere coupling: A thermostat for the tropics. *Science*, *272*(5265), 1148–1150. https://doi.org/10.1126/science.272.5265.1148
Takahashi, K., Montecinos, A., Goubanova, K., & Dewitte, B. (2011). ENSO regimes: Reinterpreting the canonical and Modoki El Niño. *Geophysical Research Letters*, *38*, L10704. https://doi.org/10.1029/2011GL047364
Taschetto, A. S., & England, M. H. (2009). El Niño Modoki impacts on Australian rainfall. *Journal of Climate*, *22*, 3167–3174. https://doi.org/10.1175/2008JCLI2589.1
Vecchi, G. A., Clement, A., & Soden, B. J. (2008). Examining the tropical Pacific's response to global warming. *Eos, Transactions American Geophysical Union*, *89*(9), 81–83. https://doi.org/10.1029/2008EO090002
Vimont, D. J., Battisti, D. S., & Hirst, A. C. (2001). Footprinting: A seasonal connection between the tropics and mid-latitudes. *Geophysical Research Letters*, *28*, 3923–3926. https://doi.org/10.1029/2001GL013435
Vimont, D. J., Battisti, D. S., & Hirst, A. C. (2003a). The seasonal footprinting mechanism in the CSIRO general circulation models. *Journal of Climate*, *16*, 2653–2667. https://doi.org/10.1175/1520-0442(2003)016<2653:TSFMIT>2.0.CO;2
Vimont, D. J., Wallace, J. M., & Battisti, D. S. (2003b). The seasonal footprinting mechanism in the Pacific: Implications for ENSO. *Journal of Climate*, *16*, 2668–2675. https://doi.org/10.1175/1520-0442(2003)016<2668:TSFMIT>2.0.CO;2
Wang, C. Z. (2001). A unified oscillator model for the El Niño-Southern oscillation. *Journal of Climate*, *14*, 98–115. https://doi.org/10.1175/1520-0442(2001)014<0098:AUOMFT>2.0.CO;2
Wang, C. Z., & Wang, X. (2013). Classifying El Niño Modoki I and II by different impacts on rainfall in Southern China and typhoon tracks. *Journal of Climate*, *26*(4), 1322–1338. https://doi.org/10.1175/JCLI-D-12–00107.1
Weisberg, R. H., & Wang, C. Z. (1997). A western pacific oscillator paradigm for the El Niño southern oscillation. *Geophysical Research Letters*, *24*, 779–782. https://doi.org/10.1029/97GL00689
Weng, H. Y., Ashok, K., Behera, S. K., Rao, S. A., & Yamagata, T. (2007). Impacts of recent El Niño Modoki on dry/wet conditions in the Pacific rim during boreal summer. *Climate Dynamics*, *29*(2–3), 113–129. https://doi.org/10.1007/s00382-007-0234-0
Weng, H. Y., Behera, S. K., & Yamagata, T. (2009). Anomalous winter climate conditions in the Pacific rim during recent El Niño Modoki and El Niño events. *Climate Dynamics*, *32*(5), 663–674. https://doi.org/10.1007/s00382-008-0394-6
Wyrtki, K. (1975). El Niño: The dynamic response of equatorial Pacific Ocean to atmospheric forcing. *Journal of Physical Oceanography*, *5*, 572–584. https://doi.org/10.1175/1520-0485(1975)005<0572:ENTDRO>2.0.CO;2
Xiang, B. Q., Wang, B., & Li, T. (2013). A new paradigm for the predominance of standing central pacific warming after the late 1990s. *Climate Dynamics*, *41*(2), 327–340. https://doi.org/10.1007/s00382-012-1427-8
Xie, F., Li, J., Tian, W., Feng, J., & Huo, Y. (2012). Signals of El Niño Modoki in the tropical tropopause layer and stratosphere. *Atmospheric Chemistry and Physics*, *12*, 5259–5273. https://doi.org/10.5194/acp-12-5259-2012
Xie, F., Li, J., Tian, W., Li, Y., & Feng, J. (2014a). Indo-Pacific warm pool area expansion, Modoki activity, and tropical cold-point tropopause temperature variations. *Science Reports*, *4*, 4552. https://doi.org/10.1038/srep04552

Xie, F., Li, J., Tian, W., Zhang, J. K., & Sun, C. (2014b). The relative impacts of El Niño Modoki, canonical El Niño, and QBO on tropical ozone changes since the 1980s. *Environmental Research Letters*, *9*, 064020. https://doi.org/10.1088/1748-9326/9/6/064020

Yang, C. X., Giese, B. S., & Wu, L. X. (2014). Ocean dynamics and tropical pacific climate change in ocean reanalyses and coupled climate models. *Journal of Geophysical Research: Oceans*, *119*, 7066–7077. https://doi.org/10.1002/2014JC009979

Yeh, S.-W., Kug, J.-S., Dewitte, B., Kwon, M.-H., Kirtman, B. P., & Jin, F.-F. (2009). El Niño in a changing climate. *Nature*, *461*, 511–514. https://doi.org/10.1038/nature08316

Yeh, S.-W., Wang, X., Wang, C. Z., & Dewitte, B. (2015). On the Relationship between the North Pacific climate variability and the Central Pacific El Niño. *Journal of Climate*, *28*, 663–677. https://doi.org/10.1175/JCLI-D-14–00137.1

Yu, J.-Y., & Giese, B. S. (2013). ENSO diversity in observations. In *CLIVAR Variations* (Vol. 11, No. 2, pp. 1–5). Washington, DC: U.S. CLIVAR.

Yu, J.-Y., Kao, H. Y., & Lee, T. (2010). Subtropics-related interannual sea surface temperature variability in the central equatorial Pacific. *Journal of Climate*, *23*, 2869–2884. https://doi.org/10.1175/2010JCLI3171.1

Yu, J.-Y., & Kim, S. T. (2011). Relationships between extratropical sea level pressure variations and the central Pacific and eastern Pacific types of ENSO. *Journal of Climate*, *24*, 708–720. https://doi.org/10.1175/2010JCLI3688.1

Yu, J.-Y., & Kim, S. T. (2013). Identifying the types of major El Niño events since 1870. *International Journal of Climatology*, *33*, 2105–2112. https://doi.org/10.1002/joc.3575

Yuan, Y., & Yang, S. (2012). Impacts of different types of El Niño on the East Asian climate: Focus on ENSO cycles. *Journal of Climate*, *25*, 7702–7722. https://doi.org/10.1175/JCLI-D-11–00576.1

Zebiak, S. E., & Cane, M. A., (1987). A model El Niño southern oscillation. *Monthly Weather Review*, *115*, 2262–2278. https://doi.org/10.7916/D8959T6K

Zhang, H., Clement, A., & Di Nezio, P. (2014). The South Pacific meridional mode: A mechanism for ENSO-like variability. *Journal of Climate*, *27*(2), 769–783. https://doi.org/10.1175/JCLI-D-13–00082.1

Zhang, P., Jin, F.-F., Li, J, & Ren, H. (2011). Contrasting impacts of two-type El Niño over the western north Pacific during boreal autumn. *Journal of the Meteorological Society of Japan*, *89*, 563–569. https://doi.org/10.2151/jmsj.2011-510

Zhang, W., & Jin, F.-F. (2012). Improvements in the CMIP5 simulations of ENSO-SSTA meridional width. *Geophysical Research Letters*, *39*, L23704. https://doi.org/10.1029/2012GL053588

Zhang, W., Jin, F.-F., & Turner, A. (2014). Increasing autumn drought over southern China associated with ENSO regime shift. *Geophysical Research Letters*, *41*, 4020–4026. https://doi.org/10.1002/2014GL060130

Zhang, W., Jin, F.-F., Zhao, J.-X., & Li, J. (2013a). On the bias in simulated ENSO SSTA meridional widths of CMIP3 models. *Journal of Climate*, *26*, 3173–3186. https://doi.org/10.1175/JCLI-D-12–00347.1

Zhang, W., Jin, F.-F., Zhao, J.-X., Qi, L., & Ren, H. (2013b). The possible influence of a nonconventional El Niño on the severe autumn drought of 2009 in southwest China. *Journal of Climate*, *26*(21), 8392–8405. https://doi.org/10.1175/JCLI-D-12-00851.1

Zhang, W., Li, J., & Jin, F.-F. (2009). Spatial and temporal features of ENSO meridional scales. *Geophysical Research Letters*, *36*, L15605. https://doi.org/10.1029/2009GL038672

Zhang, W., Li, J., & Zhao, X. (2010). Sea surface temperature cooling mode in the Pacific cold tongue. *Journal of Geophysical Research*, *115*, C12042. https://doi.org/10.1029/2010JC006501

Zhang, W., Wang, L., Xiang, B., Qi, L., & He, J. (2015). Impacts of two types of La Niña on the NAO during boreal winter. *Climate Dynamics*, *44*, 1351–1366. https://doi.org/10.1007/s00382-014-2155-z

Zhang, Y., Wallace, J. M., & Battisti, D. S. (1997). ENSO-like interdecadal variability: 1900–93. *Journal of Climate*, *10*, 1004–1020. https://doi.org10.1175/1520-0442(1997)010<1004:ELIV>2.0.CO;2